Possible stick-slip behavior before the Rausu landslide inferred from repeating seismic events

Masumi Yamada

Disaster Prevention Research Institute, Kyoto University, Uji, Gokasho, 611-0011, Japan

Jim Mori

Yuki Matsushi

• We found tiny repeating earthquakes with similar waveforms during the few hours preceding the 2015 Rausu landslide.
• This sequence is interpreted as small scale stick-slip movement leading up to the catastrophic landslide failure.
• We found that heterogeneous structure, such as asperities on the slip surface, can play an important role in the initiation of landslides.

A precursory sequence of repeating earthquakes was recorded before the Rausu landslide in Hokkaido, Japan on April 24, 2015. There were two seismic sequences with each consisting of very similar waveforms and leading up to significant landslide movements. The nearly-identical waveform shapes indicate similar source locations and mechanisms, so repeated events originated on a particular small area. This sequence is interpreted as stick-slip movement on a small patch leading up to the larger landslide failure. Our observations show that heterogeneous structure, such as asperities on the slip surface, can play an important role in the initiation of landslides, adding a new aspect to the conventional understanding of mechanisms controlling large mass movements.

1. Introduction

Seismological and geological observations of the 2015 Rausu landslide can provide new information on mechanisms of the rupture initiation. Past studies have mainly relied on spatially limited borehole coring [Schepers et al., 2001; Di Maio et al., 2010; Bievre et al., 2012], and geophysical exploration with limited resolution, such as ambient noise measurement or reflectivity methods [Burjánek et al., 2010; Grandjean et al., 2011; Bievre et al., 2012], to estimate the conditions of the undisturbed sliding surface. In this study, we focus on seismic signals with which can retrieve dynamic changes of physical parameters of landslides [Brodsky et al., 2003; Moretti et al., 2012; Yamada et al., 2013]. The benefit of using seismic signals is high-sample recording of shaking, which enables continuous observations of on-going phenomena. We used seismic signals of the Rausu landslide recorded at a very close distance (<1 km) to observe processes and properties of the slip surface immediately prior to the landslide failure. Physical phenomena associated with pre-slip, such as acoustic emissions, have been observed [Fujiwara et al., 1999; Smith and Dixon, 2014; Dixon et al., 2014], but the mechanism of rupture initiation and the contributions of slip surface conditions are not yet completely understood. For the Rausu landslide, we found two sets of repeating seismic events before the substantial mass movement. We interpret these signals as small scale stick-slip movement of the landslide and discuss the heterogeneity of the slip surface and existence of asperities that may control the landslide initiation.

2. Site description

The Rausu landslide is located on the edge of marine terrace, eastern coast of Shiretoko Peninsula, Hokkaido, northern Japan (Figures 1a and 1b). The marine terrace was eroded by surges and forms coastal cliffs with heights of 30 m. The size of the landslide is about 380 $\times$ 260 m^2 with a depth of 15-30 m and a volume of 6.2 $\times 10^5$ m^3 [Asia Air Survey Co., Ltd., 2015; Geological Survey of Hokkaido, 2015]. The displacement was 10-20 m with a rotation of 8 degrees clockwise (Figure 1c). The coastal seafloor was uplifted and emerged above the sealevel due to the buckling of the layers at the toe of the landslide (Supplementary Figure 1). There was no indication of previous mass movements at this specific site based on the original topography.

Local geology in this area consists mainly of Neogene shale with interbedded tuff layers covered by Pleistocene gravels and volcanic deposits (Figures 1c and 1d). The beddings are slightly inclined toward the coast by 10 to 20 degrees. At the landslide site, the upper part of the sliding mass is a fractured facies containing thin tuff lenses, while the lower part is hard shale with a weathered thick pumiceous tuff layer, which probably forms the slip surface of the landslide. The bottom of the coastal cliff reaches the lower hard shale, possibly close to the tuff layer.

Significant movement of the Rausu landslide started before 06:30 (JST) on April 24 based on the eyewitnesses reports, and the largest deformation occurred between 11:30

0094-8276/17/$5.00

and 16:48 on that day (Supplementary Table 1). Meteorological conditions at the site were recorded by the Automated Meteorological Data Acquisition System (AMeDAS) about 10 km north-northeast of the landslide (Figure 1b). On April 22, two days before the large displacement, the maximum temperature exceeded 15°C for the first time in the month and the snow depth decreased from 35 cm to zero within 3 days (Figure 2e and Supplementary Figure 2). A road on the landslide surface was used as a snow dump site by local people, so there was substantial water supply from melted snow. The Rausu area is very windy in winter, daily maximum of the ten minute average wind speed is 20 m/s. For a few days before the landslide, it was calm and sunny and the maximum wind speed was around 5 m/s.

3. Seismic data and methods

The seismic sequence associated with the landslide was recorded by a local short-period station at Rausu. This station is 0.85 km north of the top edge of the landslide (Figure 1b), and consists of three component one-second velocity-type sensors with 100 Hz sampling.

Figures 2a and 2b show 2 days of continuous data for the EW component band-pass filtered between 1 and 1.5 Hz, and between 2 and 4 Hz, respectively. Figure 2b clearly shows pulses of individual events with similar amplitude during two periods; around 12:00 on April 23 for about 12 hours and around 16:40 on April 24 for several minutes (Figure 2c).

We manually extracted clearly observed events (43 and 15 for the first and second sequence, respectively) and found that the shapes of the waveforms were almost identical within each sequence. Therefore, we applied a matched filtering technique to the continuous seismic data to search for more events that may be difficult to identify by eye. This technique is often used to extract individual events with similar waveforms from continuous seismic data [Gibbons and Ringdal, 2006; Peng and Zhao, 2009; Kato et al., 2012]. First, we constructed template events for the two sequences by normalizing and stacking the clearly identified events from the manual identification.

In the next step, 2 days of continuous three-component seismograms (April 23 and 24) were correlated with the template events. We computed a correlation coefficient for each component by shifting the template event by a increment of 1 sample. If the correlation coefficient exceeded 0.7 for all three components, we identified an event. To avoid duplicate detection, only the event corresponding to the maximum correlation coefficient was selected if multiple events were detected within ± 0.05 s. Both data and template events were band-pass filtered at 2 to 7 Hz to focus on the observed dominant frequencies of the seismic events.

4. Results

4.1. Estimation of the timing of large deformations

Based on the eyewitness reports, a minor seafloor uplift (less than 1 m) occurred between 07:00 on April 23 and 06:30 on April 24, and major uplift (about 10 m) occurred between 11:30 and 16:48 on April 24 (Supplementary Table 1 and 2d). The original seafloor was estimated as 1-2 m deep, since this kind of coastal bench is formed only by breaking waves at shallow depth. Therefore, the second uplift was much larger than the first one even including the depth of the seafloor.

Seismic signals from landslides tend to appear with a relatively lower frequency range due to the longer duration of the source [Moretti et al., 2012; Yamada et al., 2013], which is different from artificial human-induced noise with higher frequency content. In Figure 2a, the largest amplitude (excluding unrelated regional earthquakes) was recorded at 00:15 on April 24. This signal has a duration of 20 s and predominant frequency of 1.5 Hz (Supplementary Figure 5). The dominant amplitude is on the EW component which is parallel to the sliding direction of the land deformation. This may be related to the movement of the landslide which caused minor seafloor uplift. The sea waves also generate ambient noise of the ground, but these vibrations are much longer period (2-5 seconds in general) which is outside of our filter range.

There is another small signal around 16:46 on April 24, which is the largest amplitude in the period of possible occurrence of the major uplift. An eyewitness observed the uplifted seafloor at 16:48, and small rocks falling down from the edge of the raised area.

Based on the eyewitness reports and signals in the longer period seismic record, the timing of the minor uplift is estimated as 00:15 on April 24, and that of the major uplift is estimated as 16:46 on April 24.

4.2. Characteristics of repeating events

Applying the matched filtering technique to 2 days of continuous three-component seismograms, we extracted 106 events in the first sequence, starting from 06:00 on April 23 to 00:12 on the next day, and 23 events in the first sequence, from 16:40 to 16:47 on April 24. Note that we applied the same technique to the waveforms on April 22 and 25, but no events were detected.

The template events for the matched filtering technique are shown in Supplementary Figure 3. Note that the maximum amplitude of the EW component is normalized to one, but the relative amplitudes among the three components are preserved, so the three components have different amplitudes. Shape of the waveforms is very different between the two template events, but there are also similar characteristics.

Both events have a clear P- and S-phase, which suggests that the mechanism is some type of earthquake. The S-P time is about 0.5 s, which is in good agreement with the travel time between the landslide and station assuming a P-wave velocity 1.2 km/s and S-wave velocity 0.7 km/s. The total duration is about 4 s, including surface waves. On the other hand, the frequency contents are somewhat different for the two sequences. The dominant frequency of the largest amplitude is 2 to 3 Hz for the first sequence, and the second sequence has a lower frequency (1.5 to 2.5 Hz) for the largest amplitude. The relative amplitudes of two horizontal components are about the same for the first sequence, but the EW component of the second sequence is twice as large as the NS component.

The detailed time and amplitudes of the first sequence are shown in Figures 3a and 3b. A few very small events started after 06:00 on April 23 and the frequency increased after 12:00. The occurrence interval is roughly constant after 12:00, however, the amplitudes of the individual events increased linearly as a function of time. This characteristic suddenly changed after 21:00 on April 23. The interval between events shortened from 565 s (± 248 s standard deviation) to 204 s (± 106 s standard deviation) and the amplitudes stopped increasing at a value of about 2.5 $\times 10^{-4}$ cm/s. At the same time, more events with smaller amplitude were also activated. The small events suddenly stopped at 0:12 on April 24, followed by the minor movement of the landslide.

A second much shorter sequence of individual earthquakes contains at least 23 events from 16:40 to 16:47 on

April 24. This sequence has much shorter intervals (tens of seconds) and larger amplitudes (about 5×10^{-4} cm/s). The waveform shapes are similar among the events, but different from the first sequence (Supplementary Figures 3 and 4). The intervals between events shorten and the amplitudes decrease as a function of time (Figures 3d and 3e). At the end of the sequence, it is difficult to resolve individual events since the intervals are too short (a few seconds). These events may reflect a process directly leading up to the major movement of the landslide, which is seen as the complicated waveforms between 16:45 and 16:47 in Figure 3f.

5. Discussion

5.1. Interpretations of repeating events

Our analysis shows that there were two series of repeated seismic events that likely occurred shortly before the time of the minor and major landslide movements, respectively. The nearly-identical waveforms in a sequence indicate that the source locations and mechanisms are very similar, so we suggest that repeated small slip was occurring at a specific location on the slip surface of the landslide. With only one seismic station it is difficult to constrain the locations, however the similar waveforms indicate that the sources within a cluster are quite close. Geller and Mueller [1980] show that locations are within a quarter wavelength for the frequency of the correlated waveforms. For the 3 to 7 Hz S waves with an assumed velocity of 0.7 km/s, a quarter wavelength is 25 to 50 m. The difference of the waveforms between the first and second sequences suggests that the two sequences occurred at different locations.

The occurrence of repeating events resembles stick-slip behavior observed in rock mechanics experiments [Brace and Byerlee, 1966] and block-slider models [Burridge and Knopoff, 1967]. Similar apparent stick-slip behavior has also been observed during movement of glaciers and ice sheets at the contact between ice and bedrock [Caplan-Auerbach and Huggel, 2007; Thelen et al., 2013; Allstadt and Malone, 2014; Helmstetter et al., 2015; Lipovsky and Dunham, 2015]. Note that the maximum soil-frost depth in this area is less than 0.5 m [Kinoshita et al., 1978, @], so ice is not involved in this landslide. Stick-slip behavior implies there is a progressive shear stress accumulation, possibly caused by nearby or surrounding stable slip for this case. The stress accumulation seems to accelerate towards the large deformation, indicated by the increasing amplitudes and decreasing intervals of the events.

Another possible interpretation is that the events reflect an accelerating cracking process. However, the nearly-identical waveforms indicate that the locations of the events are located very closely together, possibly repeatedly deforming the same small patch. A cracking processes would likely extend over an area and not keep cracking the same location, and cracking events tend to migrate in space [Lockner et al., 1991; Ito and Enoki, 2007]. We do not see any changes of the waveforms indicating spatial migration, so we prefer the interpretation of repeated stick-slip behavior on the same patch.

Using the waveforms and S-P times, the largest seismic magnitude was estimated as M -1 from the velocity amplitude, based on an attenuation relationship for small earthquakes [Watanabe, 1971]. Such tiny events can only be observed if there are seismic instruments very close by (within a kilometer) and explains why this type of observation has not been previously reported for landslides. The dominant frequency of the events is 2-3 Hz for both sequences, which is much lower than expected for regular earthquakes of this size, even considering attenuation effects (corner frequency of the M -1 events is expected to be higher than 100 Hz [Abercrombie, 1995]). Therefore, these events do not fit the source scaling relations for regular earthquakes [Ide and Beroza, 2001; Oye et al., 2005; Yamada et al., 2007]. Assuming standard earthquake source models [Madariaga, 1976], the static stress drops for these events would be extremely small compared to regular earthquakes. This may be due to lower stress conditions on a landslide slip surface at very shallow depth (a few tens of meters).

We interpret the mechanism of this stick-slip as follows: the local geological structure is composed of layers of weak tuff and hard shale, so we assume the slip surface has been formed along these beddings prior to the landslide. These layers have heterogeneous thickness at the outcrop, so there may be locked and unlocked sections at the slip surface. The landslide mass seemed to be frictionally supported by these locked sections, i.e., asperities. The system has structures to generate both stick-slip movement (at locked sections) and more conventional stable sliding (at unlocked sections). In the creeping stage before the catastrophic collapse, the movement of a mass is not governed by the friction of the entire sliding surface, as conventionally interpreted, but controlled by locked sections with relatively small area. The repeated events which seems to occur at the same place is an evidence of a stick-slip movement at this locked section.

5.2. Mechanisms of the landslide movement

The beginning of the movement of the Rausu landslide process may be associated with the local weather conditions. When the air temperature rose, the water infiltration by snow melting increased the pore pressure on the slip surface. The raised pore pressure decreased the friction on the slip surface and likely initiated the process leading to the landslide. In the long term, the wave erosion contributes to destabilize the coastal cliff. The strong wind-induced wave in the winter eroded the foot of coastal cliff by excavating the weak tuff layers. However, in the short term, the wind was not so strong on the day of landslide, so that the melt-water infiltration was the main trigger of the movement.

The differences in the characteristics between the first and second repeating events may also be related to the landslide mechanism. In the first sequence, the amplitudes of events linearly increase as a function of time, but the occurrence interval is roughly constant. This sequence continues more than 12 hours and suddenly stops. The increasing amplitudes of the events may be an indication of an increase in the movement during a period of stable sliding of the undisturbed slip surface. A locked patch (asperity) on the landslide surface may have been broken during the first mass movement associated with the minor uplift.

A possible seismic signal of the first minor uplift is a smaller amplitude signal for 13 s then a larger amplitude for 4 s at 0:15 (Supplementary Figure 3). This cannot be a normal earthquake signal, since the frequency content suggests that the event should be relatively large, greater than M4, but similar signals are not recorded any other nearby stations. Therefore, this signal has to be an event very close to the seismic station, and with a long duration. The waveform may be interpreted as a long duration sliding phase followed by a short stopping phase.

In the second repeating event sequence, the amplitudes and intervals between events decrease as a function of time. This sequence continued less than 10 minutes and appears to indicate an accelerating process, suggesting that the system became unstable. The seismic signal of the major movement is not as clear as the first movement, and has very complicated waveforms. One possible interpretation is that the velocity of the movement was slower compared to the first movement, even though the total displacement (inferred from the observed uplift) was larger.

The occurrence rate of events during the first sequence changes abruptly after 21:00. The time corresponds with the arrival of seismic waves from a minor earthquake that occurred at a distance of 320 km (Mj4.4, 0.0075 cm/s and 0.209 cm/s^2 at the RAUSU station) at 21:23:43 (Figure 2). It is possible that the light shaking from this external event affected the landslide process if the system was under a very delicate balance.

6. Conclusions

We found a precursory sequence of repeating earthquakes recorded before the Rausu landslide in Hokkaido, Japan on April 24, 2015. There were two seismic sequences, each consisting of very similar waveforms and leading up to significant landslide movements. The nearly-identical waveform shapes indicate similar source locations and mechanisms, so repeated events originated on a particular small area. This sequence is interpreted as stick-slip movement on a small patch leading up to the larger landslide failure. This is one of the first observations suggesting that small scale structure, such as asperities on the slip surface, play an important role in controlling the motion of a sliding mass.

The continuous seismic signal provides information of the on-going phenomena, and reveals aspects of the mechanism of rupture initiation, which is not possible in the conventional geological approach. The study of heterogeneous surface structure by seismic signals will add a new aspect to the traditional explanations of mass movements and collapse prediction. Specific seismic signals generated from landslides may be an indicator of small scale sliding at asperities, which represent precursors to catastrophic slope failure. Recently, potential landslide surfaces can be extracted with high-resolution topographic data. For a better understanding of the initiation of rupture and structure of sliding surfaces, we need to install sensors close to potential slip surfaces to fully capture the complete range of movements leading up.

References

Abercrombie, R. E. (1995). Earthquake source scaling relationships from -1 to 5 M_L using seismograms recorded at 2.5 km depth. *J. Geophys. Res. Solid Earth*, 100(B12):24015–24036.

Allstadt, K. and Malone, S. D. (2014). Swarms of repeating stick-slip icequakes triggered by snow loading at mount rainier volcano. *J. Geophys. Res. Earth Surf.*, 119(5):1180–1203.

Asia Air Survey Co., Ltd. (2015). 2015 April Landslide in Horomoe, Rausu, Hokkaido prefecture, https://www.ajiko.co.jp/article/detail/ID52LX8TT3L/. Accessed 10 August 2015, *(in Japanese)*.

Bievre, G., Jongmans, D., Winiarski, T., and Zumbo, V. (2012). Application of geophysical measurements for assessing the role of fissures in water infiltration within a clay landslide (trieves area, french alps). *Hydrol. Processes*, 26(14):2128–2142.

Brace, W. and Byerlee, J. (1966). Stick-slip as a mechanism for earthquakes. *Science*, 153(3739):990–992.

Brodsky, E., Gordeev, E., and Kanamori, H. (2003). Landslide basal friction as measured by seismic waves. *Geophys. Res. Lett.*, 30(24):2236.

Burjánek, J., Gassner-Stamm, G., Poggi, V., Moore, J. R., and Fäh, D. (2010). Ambient vibration analysis of an unstable mountain slope. *Geophys. J. Int.*, 180(2):820–828.

Burridge, R. and Knopoff, L. (1967). Model and theoretical seismicity. *Bull. Seismol. Soc. Am.*, 57(3):341–371.

Caplan-Auerbach, J. and Huggel, C. (2007). Precursory seismicity associated with frequent, large ice avalanches on iliamna volcano, alaska, usa. *J. Glaciol.*, 53(180):128–140.

Di Maio, C., Vassallo, R., Vallario, M., Pascale, S., and Sdao, F. (2010). Structure and kinematics of a landslide in a complex clayey formation of the italian southern apennines. *Eng. Geol.*, 116(3):311–322.

Dixon, N., Spriggs, M., Smith, A., Meldrum, P., and Haslam, E. (2014). Quantification of reactivated landslide behaviour using acoustic emission monitoring. *Landslides*, pages 1–12.

Fujiwara, T., Ishibashi, A., and Monma, K. (1999). Application of acoustic emission method to shirasu slope monitoring. In *Proceedings of international symposium on slope stability engineering, Matsuyama*, pages 147–150.

Geller, R.J. and Mueller, C.S. (1980). Four similar earthquakes in central California. *Geophys. Res. Lett.*, 7 (10):821–824.

Geological Survey of Hokkaido (2015). Landslide occurred on Horomoe beach in Rausu, http://www.hro.or.jp/list/environmental/research/gsh/information/topics/ Accessed 10 August 2015, *(in Japanese)*.

Gibbons, S. J. and Ringdal, F. (2006). The detection of low magnitude seismic events using array-based waveform correlation. *Geophys. J. Int.*, 165(1):149–166.

Grandjean, G., Gourry, J.-C., Sanchez, O., Bitri, A., and Garambois, S. (2011). Structural study of the ballandaz landslide (french alps) using geophysical imagery. *J. Appl. Geophys.*, 75(3):531–542.

Helmstetter, A., Nicolas, B., Comon, P., and Gay, M. (2015). Basal icequakes recorded beneath an alpine glacier (glacier d'argentire, mont blanc, france): Evidence for stick-slip motion? *J. Geophys. Res. Earth Surf.*, 120(3):379–401.

Ide, S. and Beroza, G. C. (2001). Does apparent stress vary with earthquake size? *Geophys. Res. Lett.*, 28(17):3349–3352.

Ito, K. and Enoki, M. (2007). Acquisition and analysis of continuous acoustic emission waveform for classification of damage sources in ceramic fiber mat. *Materials transactions*, 48(6):1221–1226.

Kato, A., Obara, K., Igarashi, T., Tsuruoka, H., Nakagawa, S., and Hirata, N. (2012). Propagation of slow slip leading up to the 2011 mw 9.0 tohoku-oki earthquake. *Science*, 335(6069):705–708.

Kinoshita, S., Fukuda, M., and Yahagi, Y. (1978). Distribution of frost penetration depth of the ground in hokkaido. *Journal of Natural Disaster Science Information Analysis*, 5:10–15. *(in Japanese)*.

Lipovsky, B. P. and Dunham, E. M. (2015). Tremor during ice stream stick-slip. *The Cryosphere Discussions*, 9:5253–5289.

Lockner, D., Byerlee, J., Kuksenko, V., Ponomarev, A., and Sidorin, A. (1991). Quasi-static fault growth and shear fracture energy in granite. *Nature*, 350(6313):39–42.

Madariaga, R. (1976). Dynamics of an expanding circular fault. *Bull. Seismol. Soc. Am.*, 66(3):639–666.

Moretti, L., Mangeney, A., Capdeville, Y., Stutzmann, E., Huggel, C., Schneider, D., and Bouchut, F. (2012). Numerical modeling of the mount steller landslide flow history and of the generated long period seismic waves. *Geophys. Res. Lett.*, 39:L16402.

Oye, V., Bungum, H., and Roth, M. (2005). Source parameters and scaling relations for mining-related seismicity within the pyhäsalmi ore mine, finland. *Bull. Seismol. Soc. Am.*, 95(3):1011–1026.

Peng, Z. and Zhao, P. (2009). Migration of early aftershocks following the 2004 parkfield earthquake. *Nat. Geosci.*, 2(12):877–881.

Schepers, R., Rafat, G., Gelbke, C., and Lehmann, B. (2001). Application of borehole logging, core imaging and tomography to geotechnical exploration. *Int. J. Rock Mech. Min. Sci.*, 38(6):867–876.

Smith, A. and Dixon, N. (2014). Quantification of landslide velocity from active waveguide-generated acoustic emission. *Can. Geotech. J.*, 52(4):413–425.

Thelen, W. A., Allstadt, K., De Angelis, S., Malone, S. D., Moran, S. C., and Vidale, J. (2013). Shallow repeating seismic events under an alpine glacier at mount rainier, washington, usa. *J. Glaciol.*, 59(214):345–356.

Watanabe, A. (1971). Determination of earthquake magnitude at regional distance in and near japan. *Zisin (J. Seismol. Soc. Japan)*, 24:189–200.

Yamada, M., Kumagai, H., Matsushi, Y., and Matsuzawa, T. (2013). Dynamic landslide processes revealed by broadband seismic records. *Geophys. Res. Lett.*, 40(12):2998–3002.

Yamada, T., Mori, J. J., Ide, S., Abercrombie, R. E., Kawakata, H., Nakatani, M., Iio, Y., and Ogasawara, H. (2007). Stress drops and radiated seismic energies of microearthquakes in a south african gold mine. *J. Geophys. Res. Solid Earth*, 112(B3).

M. Yamada, Kyoto University, Uji, Gokasho, 611-0011, Japan (masumi@eqh.dpri.kyoto-u.ac.jp)

Acknowledgments. We acknowledge the National Research Institute for Earth Science and Disaster Prevention (NIED) and Japan Meteorological Agency (JMA) for the use of seismic data. Meteorological data was obtained from the JMA website (http://www.data.jma.go.jp/obd/stats/etrn/index.php). High-resolution DEM data were provided by the Asia Air Survey Co., Ltd. Dr. Shintaro Yamasaki in Kitami Institute Technology gave us the landslide information and meaningful discussion. We thank Rausu town hall and Mr. Shuichi Hamana in Rausu for providing photos of the landslide. We thank Niels Hovius and anonymous reviewer for many helpful comments on the paper. We used generic mapping tools (GMT) to draw the figures.

Figure Captions

Figure 1: Map and digital elevation model. (a) Map of Japan showing the location of landslide. (b) Map of Shiretoko peninsula with location of the landslide. Seismic stations are shown with triangles, and a meteorological station (AMeDAS) is shown with an open circle. (c) Digital elevation model of the landslide constructed from airborne LiDAR topographic surveys. (d) Geological section of the landslide along X-Y in 1c.
Figure 2: Two days continuous seismic waveforms. (a-b) EW component seismograms at RAUSU station, band-pass filtered with the window of 1 to 1.5 Hz and 2 to 4 Hz, respectively. Vertical gray bars are times of unrelated regional earthquakes. (c) Three-component amplitude of events. (d) Time of eyewitness reports, giving constraints on landslide occurrence timing. (e) Snow depth and temperature at the AMeDAS Rausu station.
Figure 3: The first (a-c) and second (d-f) sequences of small earthquakes. (a,d) Three-component amplitude of events. The dotted line indicates a local earthquake at 21:23:43. (b,e) Number of events identified by the matched filtering. (c,f) EW component of velocity at RAUSU station band-pass filtered 2 to 7 Hz.

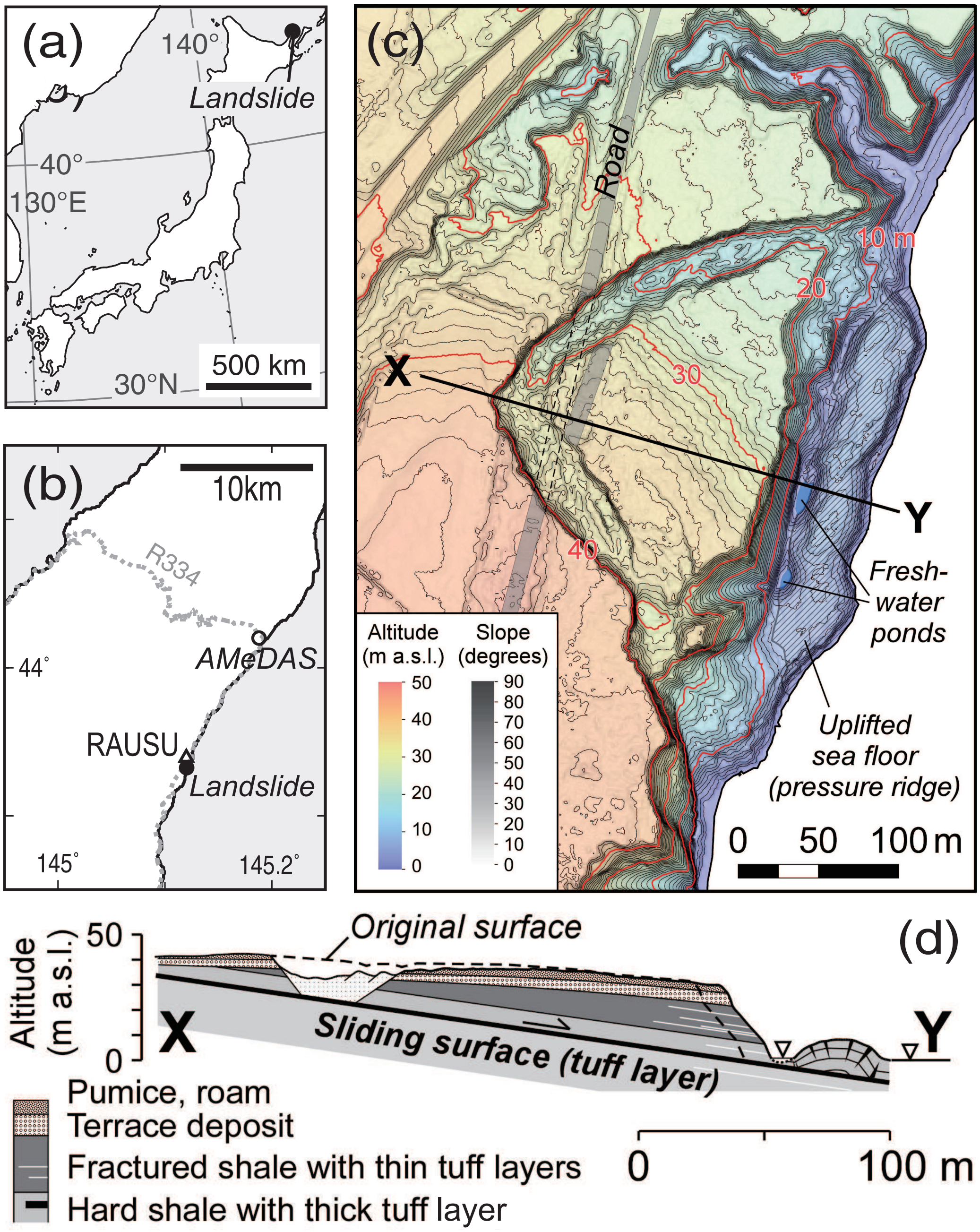

Figure 1.

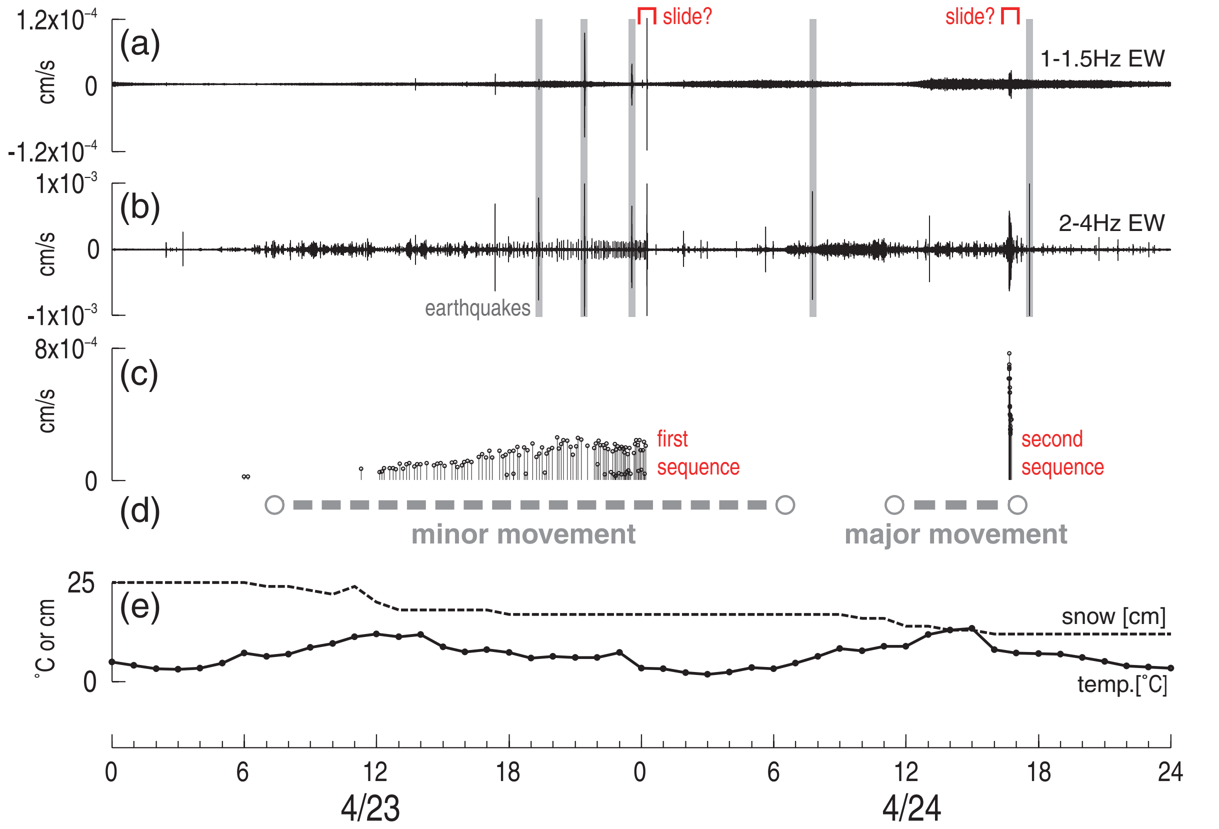

Figure 2.

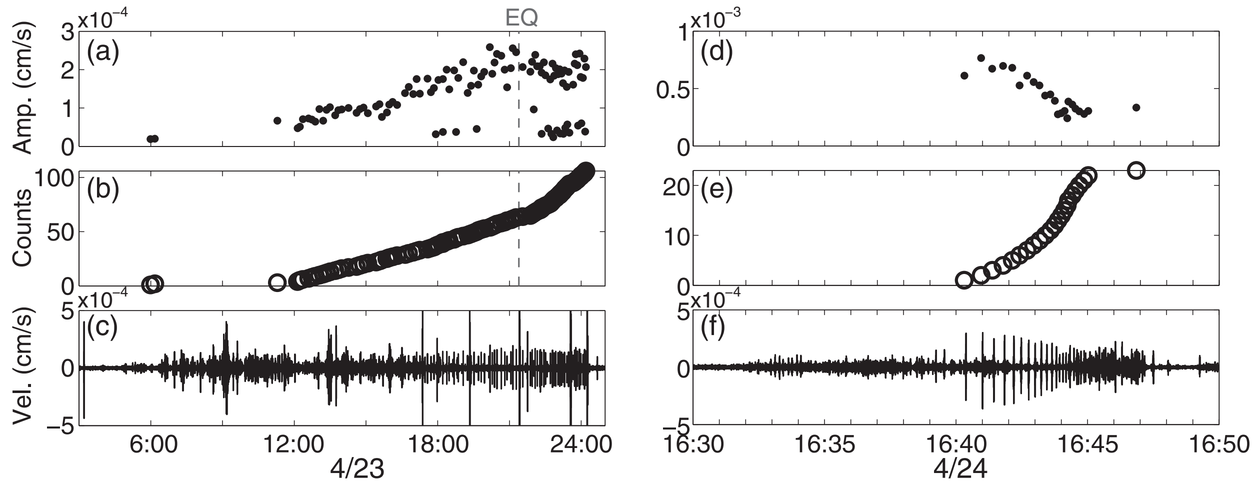

Figure 3.